Advances in Science and Technology Research Journal

Advances in Science and Technology Research Journal, 2026, 20(5), 254–267
https://doi.org/10.12913/22998624/216335
ISSN 2299-8624, License CC-BY 4.0

Received: 2025.12.05
Accepted: 2026.03.15
Published: 2026.04.01

Implementation of a multi-sensor platform for resource localization using ultra-wideband and time-of-flight measurement methods

Michał Styła[1], Dominik Gnaś[2], Adam Bogusz[2], Dariusz Wójcik[2,3], Przemysław Adamkiewicz[1,3], Tomasz Rymarczyk[2,3], Paweł Kaleta[3], Monika Kulisz[4], Grzegorz Kłosowski[4*]

[1] Research and Development Center of Information Technologies (CBRTI), Aleja Tadeusza Rejtana 67, 35-326 Rzeszów, Poland
[2] Research & Development Centre Netrix S.A., ul. Związkowa 26, 20-704 Lublin, Poland
[3] WSEI University, ul. Projektowa 4, 20-209 Lublin, Poland
[4] Lublin University of Technology, ul. Nadbystrzycka 38D, 20-618 Lublin, Poland
* Corresponding author's e-mail: g.klosowski@pollub.pl

ABSTRACT

The work addresses the design and implementation of a miniature, energy-efficient multi-sensor platform for indoor asset tracking in warehouse and production environments. The proposed system localizes objects using time-based distance measurement methods, namely two way ranging (TWR) and time of flight (ToF) markers obtained from ultra-wideband (UWB) transmissions. Custom four-layer PCB tags and anchors populated predominantly with 0201 components enable compact integration of the UWB transceiver, Bluetooth interface and an environmental sensing module (temperature, humidity and pressure), while power over ethernet (PoE) support on the anchor side simplifies deployment in industrial facilities. Motion-triggered activation based on an on-board accelerometer allows distance measurements to be initiated only when significant movement occurs, which reduces energy consumption and limits data acquisition to events relevant for logistics processes. A calibration and test campaign carried out in a 28 m indoor corridor demonstrates that, after antenna-path correction, raw ToF-based distance estimates typically remain within 10–20 cm of the ground truth for most control points, with larger deviations attributable to multipath propagation. To further stabilize the readings, a one-dimensional Kalman filter is applied to distance time series, reducing the mean RMS error from 81.19 cm to 25.63 cm (68.4% reduction) and improving the signal-to-noise ratio by approximately 10 dB. The results confirm that the proposed hardware–software architecture can provide accurate, energy-aware UWB localization suitable for integration with warehouse management and production control systems.

Keywords: process automation, multi-sensor platform, asset tracking, indoor positioning system, temporal distance measurement.

INTRODUCTION

An effective asset management system poses a major technological challenge due to the ever-increasing demands for complexity in the solution. Increasingly, issues related to the distribution of materials, whether in storage or production, are linked to radio location systems, which are expected to provide ever greater tracking accuracy and operate for several months or even years on a single galvanic cell. Commonly available energy sources, such as lithium cells, are not technologically adapted to the type of work imposed on them by RF transmitters. In addition, these devices should be extremely small in size, allowing for non-invasive and comfortable attachment to even the smallest details/objects. The phenomenon of electromagnetic radiation itself is fraught

with many side effects of a wave nature, such as multipath propagation or sources of interference that constantly increase noise levels in urban areas. Therefore, the activities presented in this paper focused not only on creating a typical solution for WMS systems, but also on work aimed at eliminating or significantly reducing their greatest weaknesses. Solutions using combined methods of time-based radio distance measurement and a digital layer responsible for communication have a significant advantage over competing solutions based on measuring the power of the received signal [1]. However, this does not mean that such an approach eliminates all parasitic effects and creates new challenges in the field of transmitter calibration, device repeatability, and maintaining good performance parameters, especially in industrial environments [2–4].

Contemporary indoor tracking pipelines use nonlinear Bayesian filters such as the EKF, UKF, and CKF together with tightly coupled fusion of UWB and IMU data. Inertial information improves transient behavior and maintains trajectory continuity during packet loss. Because the platform already includes an accelerometer, adopting a tightly coupled design would strengthen continuity and robustness in the presence of interference [5,6].

The system structure consists of two groups of devices comprising reference points, known as anchors, and localized points, known as tags. The task of a tag attached to an asset is to actively communicate with all reference points within the range of the UWB (Ultra WideBand) transmitter. This makes it the initiator of TWR transmission aimed at obtaining output data for calculating the distance between devices (ToF). The main operations performed by these devices are presented in the functional diagram in Figure 1. The use of such a measurement method without the use of a global synchronization signal or other external conditioning requires the implementation of a transmission activation control system on the UWB transmitter itself. Such a complex pair is the smallest cell forming the system.

When comparing UWB architectures, we focus on energy efficiency (accuracy per joule). Asynchronous TDoA can reduce the tag's on-air time compared with SS/DS-TWR for similar update rates. In addition, the IEEE 802.15.4z PHY choice (HRP vs. LRP) affects receiver complexity and instantaneous current peaks, which directly impacts battery lifetime claims [7].

After successful acquisition, the data collected by the anchors can be pre-formatted and distributed throughout the entire local network of the building. The actual location is determined in a computing cluster, and its results are presented in graphical form, e.g., in a three-dimensional visualization of the building [8,9].

Front-ends increasingly deploy learning-based NLOS gates trained on CIR-derived features to flag or compensate bias prior to filtering, which improves stability in cluttered layouts;

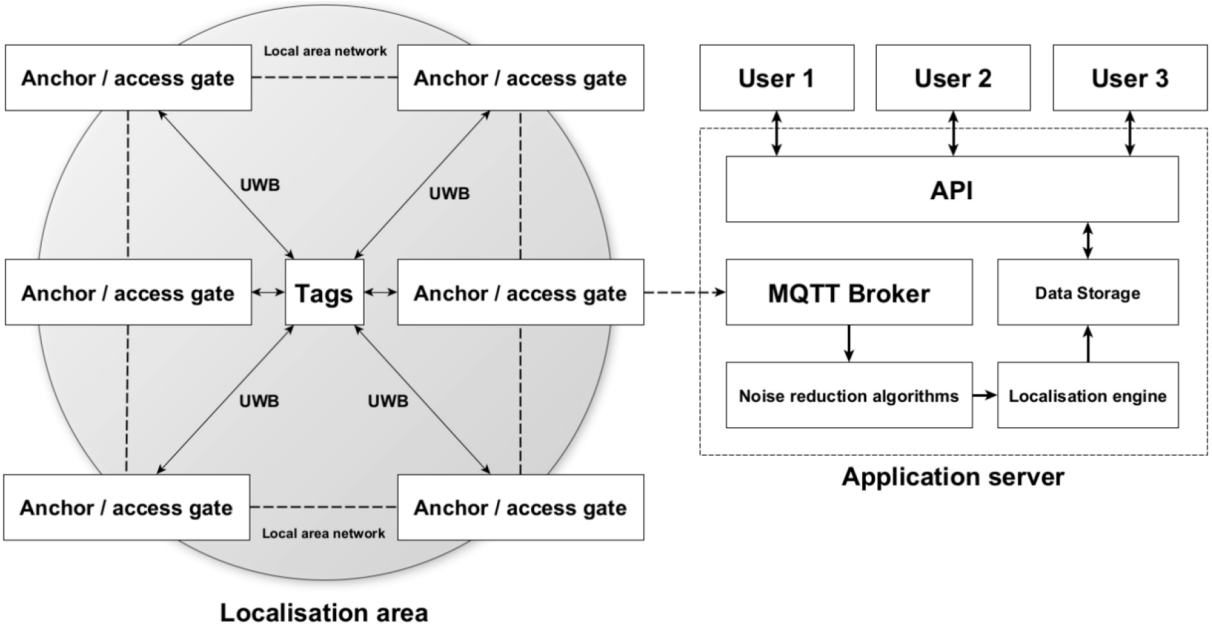

Figure 1. Block diagram of a system designed to operate ultra-wideband transceivers and track assets

inserting such a gate aligns the estimation chain with prevailing practice [10,11]. Reporting conventions in recent IPS/UWB work foreground distributional accuracy (CDF, P95) and motion-aware trials, often with ablations contrasting linear vs non-linear filters and fixed vs adaptive noise, and these conventions provide useful guidance for analyzing error distributions, tail-risk and latency in practical evaluation campaigns [7,12].

Contextually to asset integrity and logistics, non-destructive testing (NDT) shows a parallel shift toward digital, non-contact modalities and integrated data flows: alongside established UT/PAUT/TOFD[13], DR/CR[14], ECT/ECA[15–17], MT/PT, thermography and AE [18], tomography-class imaging (XCT/μCT [19], ultrasound tomography [20,21], electrical tomography [22,23], OCT[24,25]) is widely adopted each with distinct trade-offs (e.g., radiography's shielding burden; PT/MT's consumables; thermography's environment sensitivity). Recent surveys on industrial condition monitoring and structural health monitoring emphasise thermography, shearography, microwave and tomography-based techniques combined with data-centric workflows that reduce consumables, inspection time and downtime, which is directly relevant for designing low-touch, power-aware sensing platforms in production and logistics environments. Similar tendencies are reported in impedance and capacitance tomography, where learning-enhanced reconstruction pipelines bring measurable reductions in computation time and resource usage while maintaining diagnostic performance [26,27]. These results support the development of sustainable, data-driven inspection chains and offer methodological analogies for ultra-wideband indoor asset tracking systems.

Complementary advances in industrial measurement and control further illustrate this trend. Studies on electrical resistance and capacitance tomography have shown that, when combined with dedicated image reconstruction and machine learning algorithms, such techniques enable quantitative assessment of low-conductivity media and two-phase gas–liquid flows under demanding process conditions [16,17]. Other works on refined sensor design and adaptive control algorithms indicate that metrological robustness and operational efficiency can be significantly improved in industrial flow measurement and aeration systems [28,29]. Together, these results underline a broader shift towards intelligent, model-based sensing and control in mechanical and process engineering.

Despite these advances, there is still a noticeable gap between low-level radio/localisation techniques and the requirements of asset-intensive logistics environments. Many existing UWB-based indoor positioning systems either sacrifice update rate and robustness to meet multi-month power budgets, or deliver accurate trajectories at the cost of bulky hardware, frequent maintenance, or limited scalability in cluttered industrial buildings. In practice, operators must still tolerate missing or delayed asset information, manual reconciliation steps, and non-trivial integration effort with warehouse management systems. This motivates the development of location platforms that are simultaneously energy-aware, resilient to interference, and natively compatible with digital asset-management workflows.

The aim of this work is to design, implement and experimentally evaluate an ultra-wideband asset tracking platform that uses time-based ranging with motion-triggered tag activation and statistical filtering of distance time series to improve indoor localization accuracy in a representative indoor environment, while remaining compatible with long-lifetime, low-maintenance operation on resource-constrained tags.

In this context, a compact hardware architecture for UWB anchors and tags is proposed and implemented. It is based on four-layer PCBs populated predominantly with 0201 components, integrates UWB, Bluetooth and environmental sensing, and enables energy-aware operation with motion-triggered activation on the tag side and power over ethernet (PoE) on the anchor side. A tag-initiated two-way ranging protocol and data flow are designed, in which motion-conditioned UWB measurements are collected at anchors and forwarded via the building network to a computing cluster, where only current coordinates and historical traces are stored to support warehouse and production management. A calibration and experimental evaluation campaign in a real indoor corridor environment is carried out, characterizing distance measurement errors, repeatability across devices and the impact of multipath, and providing a practical correction procedure for proprietary antenna paths. In addition, a one-dimensional Kalman filter for distance time series is implemented and evaluated, achieving on average a 68.4% reduction in RMS error and an improvement of approximately 10 dB in

SNR, with the limitations of this approach and future extensions towards adaptive and nonlinear filtering being discussed. Finally, analogies to digital, tomography-inspired diagnostic chains from non-destructive testing and impedance/capacitance tomography are explored, showing how their data-centric and energy-aware design patterns can inform the architecture of indoor asset tracking platforms.

MATERIALS AND METHODS

To fulfill the designated localization tasks, a series of proprietary structural solutions were designed and implemented, including both anchors and ultra-wideband signal tags. Despite sharing a common radio component, consisting of UWB transceivers and Bluetooth (in an auxiliary form), they are specialized to perform specific roles. This primarily concerns the power supply and the type of data that will be transmitted between the transmitter and receiver, and between the receiver and the computing cluster [30].

The anchor is a reference point in space for all ultra-wideband tags. It is also an access point to the building's local network through which data is transferred outside the UWB network. It consists of a four-layer FR4 laminate with maximum dimensions of 48 mm in width and 71 mm in height. The outer copper layers are dedicated to the distribution of radio and control signals, while the two inner layers are dedicated to the power supply networks for individual modules. For maximum miniaturization of the platform, 90% of the passive components are 0201 in imperial scale (0603 in metric scale). This allowed for maximum packing of microcontroller peripherals and controllers in QFN packages. Due to the high concentration of components and their close proximity to transmission lines and RF impedance matching circuits, small, high-performance ceramic antennas with high resistance to PCB interference were used.

The anchor's master control unit is a high-performance STM32F746VGT6 microcontroller equipped with an ARM Cortex-M7 core with a maximum clock speed of 216 MHz. This provides sufficient computing resources for simultaneous reception and processing of information contained in radio signals and handling Ethernet connections. Direct communication with the UWB network is provided by the DWM1000 RF front-end controlled via the SPI interface. A WSoC (wireless system on a chip) nRF52832 microcontroller connected to the PCB central unit via a UART serial bus has also been added to the platform in a supporting role. It can operate independently of the rest, transmitting additional information outside the ultra-wideband network transmission channels. Connection to the local network is provided by a standard 4-pair twisted pair cable terminated with an RJ-45 connector. Additionally, it also serves as a power supply. This is due to the use of a configuration that includes PoE (Power over Ethernet). The maximum voltage of 48 V, after being fed to the isolation transformer, is reduced to 5 V and then distributed between the modules or further reduced to other logic levels. Issues related to the management of connections and power supply of this type are handled with the help of an external LAN8742A Ethernet controller. To ensure maximum stability of PCB operation, the RF, control, and power supply components have been spaced as far apart as possible. The 3D visualization of the laminate shown in Figure 2.

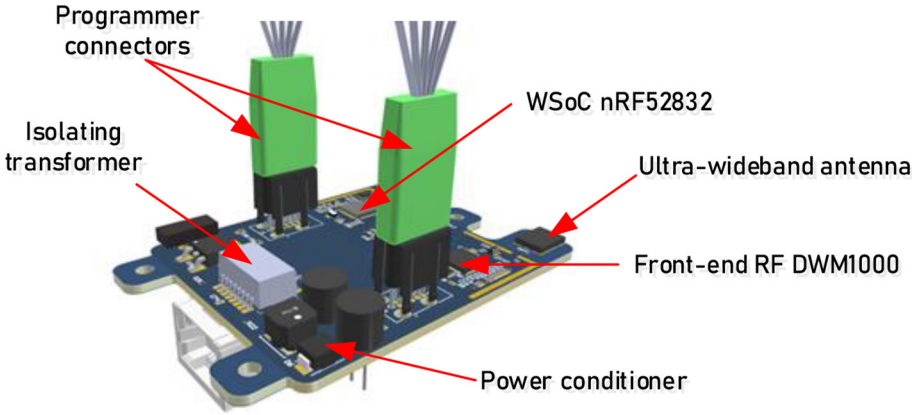

Figure 2. Three-dimensional visualization of a proprietary ultra-wideband anchor

The ultra-wideband tag was made using the same concept as the anchor. It consists of a four-layer FR4 laminate with an identical layer configuration but a significantly smaller total area (43 mm wide and 42 mm high), allowing it to be easily attached to as many objects as possible. The layout of the individual modules is also similar. The power supply and radio components have been moved to opposite edges of the PCB. The central part is occupied by control module components and a multi-sensor platform used to monitor environmental parameters (storage conditions) and condition the tag's activation. Almost all passive components used on the PCB are 0201 size. All critical sectors of the PCB are surrounded by exposed ground planes allowing for the installation of additional shielding boxes. This applies primarily to the separation of control modules and active RF parts. In addition, the entire surface of the laminate is covered with potential equalization points, and the RF transmission lines are covered with shielding tunnels. The technical solutions for interference immunity are the same for both devices [31].

Unlike the anchor, the nRF52832 connected to the DWM1000 RF front-end via an SPI interface plays the primary role in controlling the device. The rest of the components, mostly environmental sensors, are connected via a common I2C bus. This group includes the SHT21 temperature and humidity sensor and the LPS33HWTR pressure sensor. The same interface also includes FRAM non-volatile memory and an ICM-42605 accelerometer with advanced motion detection and recognition features. The latter allowed for the implementation of the WoM (Wakeup on Motion) function, which, in combination with the advanced power saving and sleep modes of the nRF52832, improved the energy efficiency of the platform. This significantly extended the total operating time on a single cell. Depending on the specifics of the asset storage location, recognition of specific types of movement can also be added. The entire tag power supply network is controlled by the nPM1100 PMIC (power management integrated circuits) chip. Due to the specific nature of this chip, the other components are powered by a reduced voltage of 3 V. The PCB is designed to work with a 1500 mAh lithium-polymer battery. For safety reasons, a thermal protection device has been placed on the PCB. The appearance of the device ultra-wideband anchor and ultra-wideband tag is shown in Figure 3.

Anchor placement was planned to provide continuous coverage of the test area while maintaining favorable geometry for ranging. In the considered warehouse-like layout, anchors were installed at elevated positions and distributed along the area with an approximate spacing of about 7 m, which ensured that the entire zone remained within the operational range of multiple anchors. In aisle-dominated environments, such spacing and placement at corridor intersections helps maintain overlap between neighboring anchors and mitigates local NLOS sections.

The data is collected via the TWR (two way ranging) radio procedure. The calculated time stamps (both partial and final) are transported to the anchor, from where the information about the

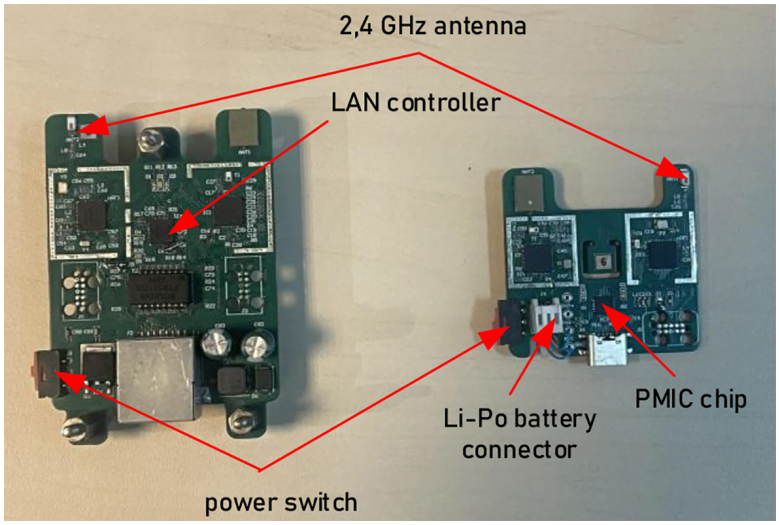

Figure 3. View of the prepared devices: ultra-wideband anchor (left) and ultra-wideband tag (right)

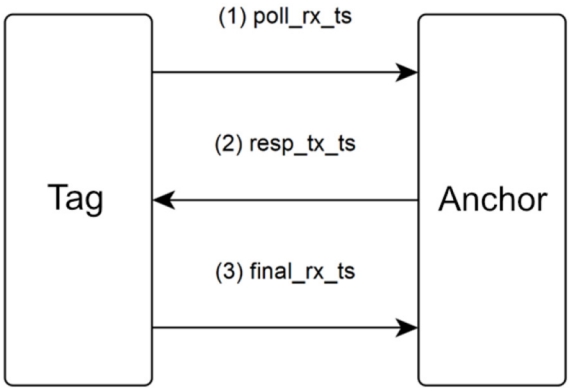

Figure 4. Basic TWR communication scheme between UWB tag and UWB anchor

distance between the devices is signed and distributed via the building's local network. In order to optimize the system's performance and save storage space, it was decided to store only the current coordinates of the tags and the historical trace, e.g. for production management and record keeping. The exact principle of operation of the locator is shown in Figure 4 [32,33].

The initiator of transmission in the presented system is always a device that is moved and attached to the tracked asset. For energy optimization, measurement initialization is conditional on exceeding the set sensitivity threshold of the accelerometer (in all three axes). This allows the system to take into account only changes in the position of the object that are significant from the user's point of view, or to control unauthorized access to the monitored resource. From the point of view of the receiving part, this also limits activity by reducing the number of calculations (position estimation). For a stationary object, the last coordinate record will always be current. Transmission begins with the *poll_rx_ts* command, thus creating the first temporal checkpoint. The second is created on request by *poll_rx_ts* in the form of a *resp_tx_ts* response. Upon reaching the reception time marker, taking into account the bidirectional transit time, the speed of light, antenna path propagation delays, and transmitter-receiver delays, the distance between the reference point (anchor) and the tag is calculated. Due to the lack of appropriate hardware resources for the tag, the calculated values must be sent to the anchor that has a direct connection to the building's communication network. This is done as part of the *final_rx_ts* command. The implementation of the TWR method is an alternative to a global synchronization signal. Due to the large dispersion of devices in WMS systems and harsh environmental conditions affecting radio signal propagation, the selected configuration ensures better optimization of operation regardless of the architectural object covered by the operation. Devices created in accordance with this configuration have undergone a series of trials and tests to determine their radio properties. In order to enable the recording and analysis of the results obtained at early stages without increasing the complexity of the design, a digital environment was used, which allowed data acquisition via a JTAG programmer connector. A model of the virtual measurement system is presented in Figure 5 [34,35].

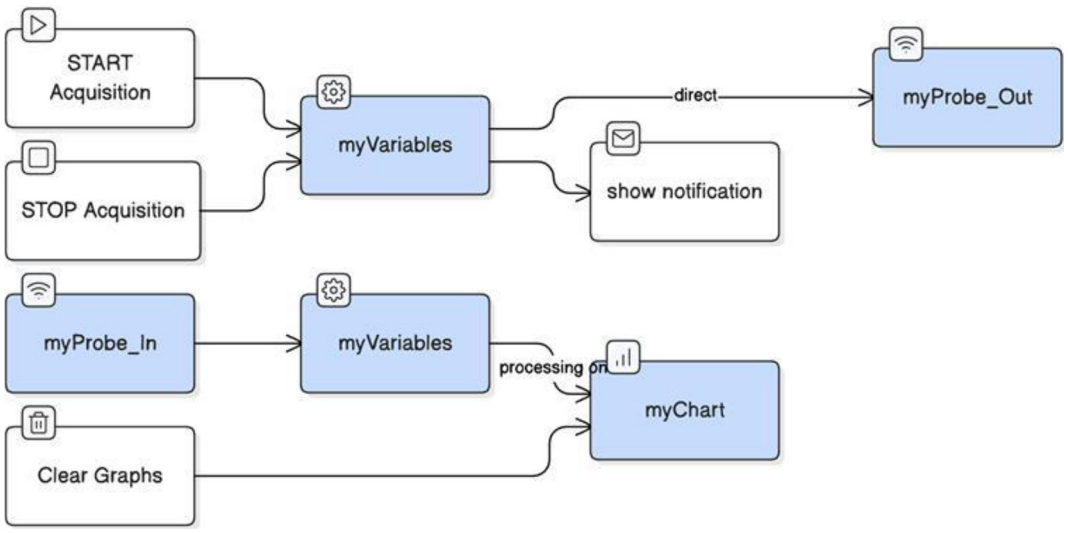

Figure 5. Virtual system for acquiring and visualizing data obtained using the ToF method (STM32Monitor environment)

The view of unfiltered data with the typical spread of values for the selected technology is shown in Figure 6. The tests were performed for the longest available corridor (28 meters) in an office building with a 1-meter increment. The value shown in the figure corresponds to the measurement at 7 meters of the track, and the maximum observable spread of values for the vast majority of the range was within 20 centimeters (without additional processing). The proprietary antenna paths required time corrections due to large differences between the measured and actual values. In the analyzed case, the same adjustment was adopted for transmission and reception (common transmission and reception path). For both the tag and the anchor, it was 0.5 nanoseconds per 15 cm. For one case measuring 250 cm (the difference between the reading and the actual distance of the tag), this was an 8.33 nanosecond correction. The time value obtained in this way was a measure of the delay resulting from signal propagation, which then had to be related to the delay calculated using a 64 MHz system clock. Using the relationship between frequency and period, 15.65 picosecond (duration of a single clock cycle for DWM1000) was obtained, which, when divided by the calculated propagation time, gave 532.3 units of system clock cycles. While maintaining the repeatability of the manufactured electronics and the components used in them, this correction can be assumed to be constant for all devices.

RESULTS

Radio tests covered many aspects of the manufactured devices, such as the stability of distance readings, operating range, and repeatability of measurements obtained using different devices. A key aspect of the system under development was the stability of the results obtained to ensure maximum location accuracy. The reference (ground-truth) distance was the physically measured separation between the tag and the anchor at each control point. The deviation was computed as and is reported in centimeters. Figure 7 shows the average deviation in centimeters from the actual distance for which the measurement was taken. With the exception of two points, i.e., 12 meters and 18 meters (measurements performed with a person present in the propagation path, causing temporary NLOS/multipath), the distance readings for calibrated devices did not exceed an error of 20 cm in a few cases and 10 cm for most control points. Errors of 80–100 centimeters were most likely the result of the parasitic effect of multipath propagation, to which the ToF method is vulnerable to a similar extent as methods using the amplitude properties of RF signals. At the indicated locations (control points), some architectural barriers could act as reflectors for RF signals, but this is difficult to avoid due to the variety of buildings in which the system can be installed. In practical deployments, local reflectors (e.g., metal

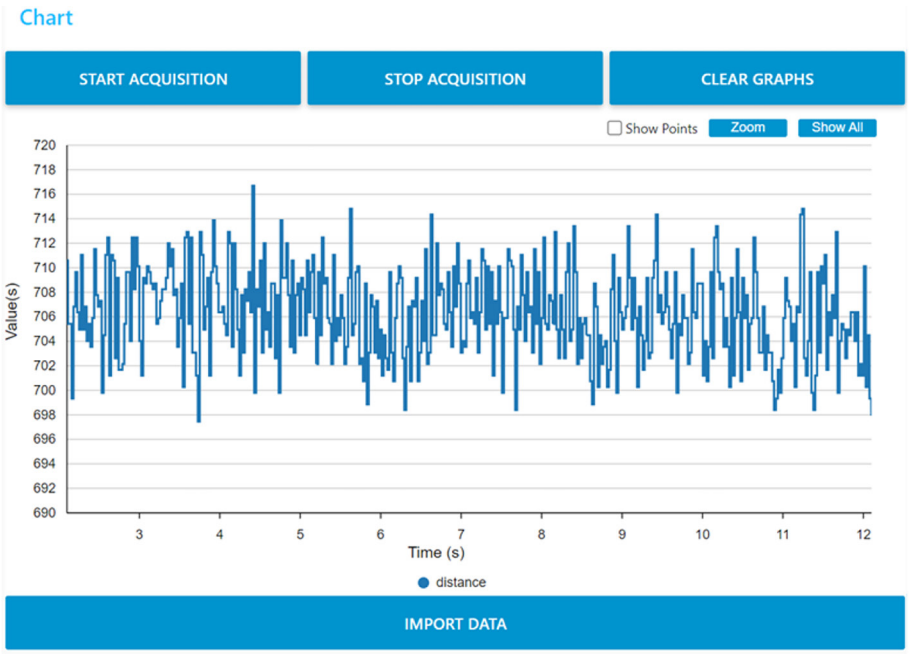

Figure 6. Measurement of the distance in centimeters between the UWB tag and the UWB anchor performed in the time domain

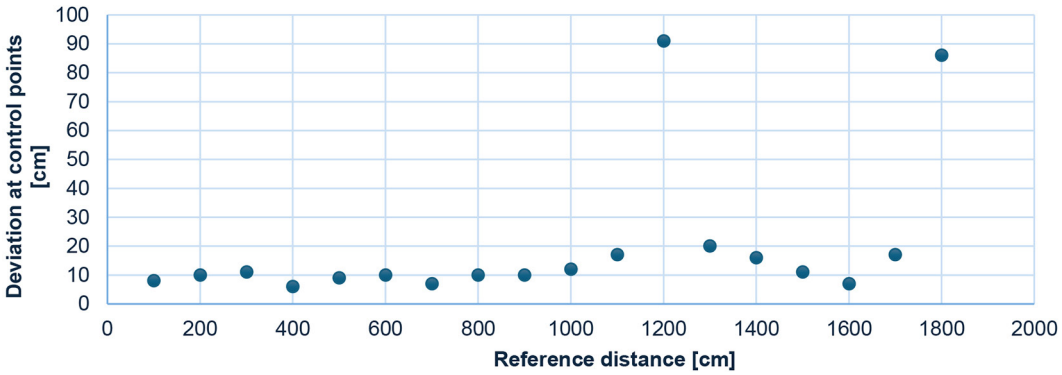

Figure 7. Differences between the distance indicated by the ToF method and the actual value at a distance of 20 meters

structures or walls) may additionally increase multipath effects. However, such conditions are difficult to avoid due to the variety of buildings in which the system can be installed. This is also confirmed by the fact that the same measurements were performed for several different devices of the same type, and the disturbances occurred in exactly the same places. Errors of this type can be eliminated by using a sufficiently large number of reference points, which makes it much easier to detect critical points [36,37].

The analysis of result variability over time is presented in Figure 8 for three different tags. The reference value in this case was 120 centimeters. At this stage, the tag prototypes were assembled manually, which is reflected in the differences between the average error values. Despite the calibration of time delays with an accuracy of single machine cycles, tag 1 tended to underestimate the result, tag 2 tended to overestimate it, while tag 3 was closest to the center, i.e., the actual value. This error will be minimized with the transition to machine assembly, which allows for greater repeatability of the manufactured device. In the case of radio devices that use the phenomenon of resonance and require strict impedance matching control, this aspect is critical to ensuring optimal performance of the location network.

Although the tag PCBs share an identical layout, the assembled RF front-end exhibits device-to-device variability due to component tolerances and placement deviations (e.g., matching-network passives and antenna-related components). Even small tolerances (e.g., 0.1–0.5%) can slightly shift the impedance match and the effective radiation efficiency, which primarily affects the link budget and therefore the achievable range and the stability of reception. The ToF/TWR distance accuracy is less sensitive to these variations than amplitude-based ranging. However, minor per-device offsets may still occur due to analog front-end differences and antenna detuning. In the final production flow, this variability is mitigated by machine assembly (improved placement repeatability) and basic RF/functional QA, followed by per-device calibration of timing delays.

To improve the accuracy of noisy distance measurements obtained from the sensor, a Kalman filter was implemented. The main goal was to achieve an improvement in signal-to-noise ratio (SNR) of at least 5 dB, with actual results showing an improvement of ~10 dB. The Kalman filter was chosen for its effectiveness in real-time noise reduction for time series data. The input data consists of distance measurements in the form of time series for which the true distance values are known. The noise characteristics include high measurement variability, including extreme outliers. The aim of the work was to reduce the noise level while preserving the true signal, assuming an improvement in SNR of at least 5 dB. The Kalman filter is an optimal recursive estimator that minimizes the mean square error for linear systems with Gaussian noise. It works in two steps. It estimates the next state based on the current state and process model, and then corrects the estimates based on new measurements. The state vector includes distance and velocity. The state transition model assumes constant velocity, and the measurement model is defined as a distance extraction matrix. The process and measurement noise covariance matrices are key parameters affecting the quality of filtering. For state vector [38–40]:

$$X_k = \left[\frac{distance}{velocity}\right] \tag{1}$$

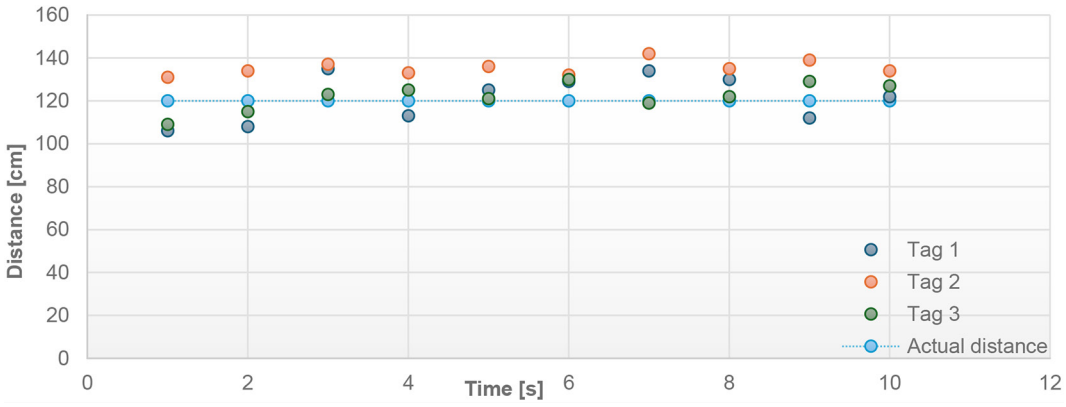

Figure 8. Variability of distance results obtained over time for three different tags of the same type and an actual distance of 120 cm

For state transition model (constant velocity):

$$F_k = \begin{bmatrix} 1 & \Delta t \\ 0 & 1 \end{bmatrix} \tag{2}$$

For measurement model:

$$\boldsymbol{H} = [1\ 0] \tag{3}$$

For process noise covariance (Q):

$$Q = \begin{bmatrix} \frac{\Delta t^4}{4} & \frac{\Delta t^3}{2} \\ \frac{\Delta t^3}{2} & \Delta t^2 \end{bmatrix} \times \sigma_a^2 \tag{4}$$

Measurement Noise Covariance (R) will be the estimated value from the measurement data.

The prediction equations for the Kalman filter involve state extrapolation and covariance matrix update. In the update step, the Kalman gain matrix is calculated, which determines the weight of the measurement in the estimate correction. The final update of the state and covariance is performed taking into account the new observation. For prediction:

$$\hat{\mathbf{x}}_{k|k-1} = \mathbf{F}_k \hat{\mathbf{x}}_{k-1|k-1} \tag{5}$$

$$\mathbf{P}_{k|k-1} = \mathbf{F}_k \mathbf{P}_{k-1|k-1} \mathbf{F}_k^T + \mathbf{Q} \tag{6}$$

For data update:

$$\mathbf{K}_k = \mathbf{P}_{k|k-1} \mathbf{H}^T (\mathbf{H} \mathbf{P}_{k|k-1} \mathbf{H}^T + R)^{-1} \tag{7}$$

$$\hat{\mathbf{x}}_{k|k} = \hat{\mathbf{x}}_{k|k-1} + \mathbf{K}_k \left(z_k - \mathbf{H} \hat{\mathbf{x}}_{k|k-1} \right) \tag{8}$$

$$\mathbf{P}_{k|k} = (\mathbf{I} - \mathbf{K}_k \mathbf{H}) \mathbf{P}_{k|k-1} \tag{9}$$

where $\hat{\mathbf{x}}_{k|k-1}$ is the a priori (predicted) state estimate at time step k, computed using measurements up to $k-1$; $\hat{\mathbf{x}}_{k-1|k-1}$ is the a posteriori (updated) state estimate at time step $k-1$; $\hat{\mathbf{x}}_{k|k}$ is the a posteriori (updated) state estimate at time step k after incorporating the measurement z_k; $\mathrm{P}_{k|k-1}$ is the a priori error covariance matrix of the state estimate at time step k; $\mathrm{P}_{k-1|k-1}$ is the a posteriori error covariance matrix at time step $k-1$; $\mathrm{P}_{k|k}$ is the a posteriori error covariance matrix at time step k; F_k is the state transition matrix that models the state evolution from k – 1 to k; Q is the process-noise covariance matrix, representing uncertainty in the assumed system model and unmodeled dynamics; z_k is the measurement vector at time step k(in this work, the UWB/ToF-based distance measurement); H is the measurement (observation) matrix that maps the state space to the measurement space; R is the measurement-noise covariance matrix, capturing the variance of the ranging noise (e.g., multipath/NLOS effects); K_k is the Kalman gain, which weights the contribution of the new measurement relative to the model prediction; I is the identity matrix of appropriate dimension.

Preliminary data processing used raw data from spreadsheets where each file corresponded to a specific true distance. The data was then combined into a single data frame for analysis. Processing included removing missing values, normalizing time, and calculating measurement errors. The Kalman filter was implemented in Python using the NumPy library for matrix operations. The Kalman filter function processes distance measurements and returns smoothed estimates. Key steps include state prediction, calculation of the prediction covariance matrix, update

based on measurement, and covariance matrix correction. The filter was applied to each group of measurements corresponding to a specific true distance. Tuning parameters, such as the process noise matrix Q and measurement noise variance R, were adjusted based on the noise characteristics for each group. For groups with a small number of measurements, a simplified approach without filtering was used. Figure 9 shows a typical reading of distance values over time (blue) compared with the result of the noise reduction filter (green), while Table 1 presents the overall performance achieved using the methods presented [41]. The mean RMS error was reduced from 81.19 to 25.63, representing an improvement of 68.4%. The signal-to-noise ratio (SNR) improved from 17.19 dB to 27.21 dB, representing an increase of 10.02 dB, significantly exceeding the target. Table 2 shows the improvement results for individual data groups up to 10 meters.

The greatest improvement in SNR was observed at a distance of 400 cm, where the

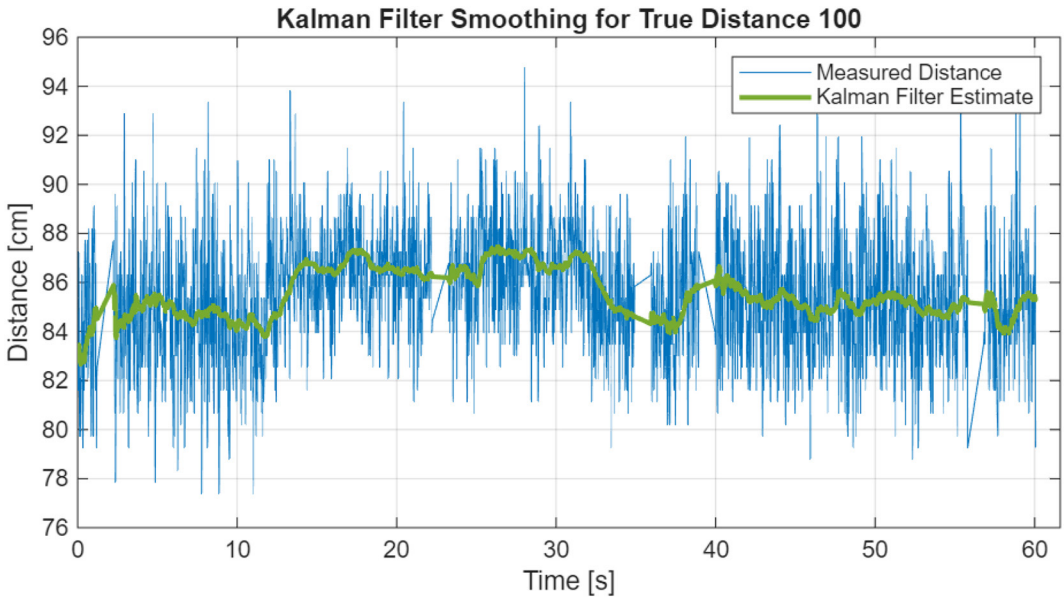

Figure 9. Stabilization of distance readings in the time domain using a Kalman filter

Table 1. Overall performance of the denoising algorithm using the example of the Kalman filter

Metric	Measured	Kalman filtered	Improvement
RMS error (cm)	81.19	25.63	68.4% Reduction
SNR (dB)	17.19	27.21	+10.02 dB

Table 2. The improvement results for individual data groups up to 10 meters

True distance (cm)	SNR (Measured, dB)	SNR (Filtered, dB)	Improvement (dB)
100	16.64	16.89	+0.25
200	3.03	18.70	+15.67
300	18.37	18.24	-0.13
400	8.63	34.30	+25.68
500	37.60	40.72	+3.12
600	42.40	54.63	+12.23
700	44.38	49.63	+5.25
800	41.45	59.53	+18.08
900	37.38	38.85	+1.47
1000	37.76	41.33	+3.57

increase was 25.68 dB. For distances of 200 cm and 800 cm, the improvement was 15.67 dB and 18.08 dB, respectively. The only case of slight deterioration was at a distance of 300 cm, where the SNR decreased by 0.13 dB, which was probably due to the suboptimal selection of the Q and R parameters. This could have been caused by possible signal reflections generating false signals resulting from the geometry of the measurement system and its location in the laboratory. The results comparing raw measurements with smoothed Kalman filter estimates clearly show noise reduction and signal trend preservation. For example, for a distance of 800 cm, the filter effectively eliminated extreme outliers while maintaining smoothness.

DISCUSSION

The experimental results confirm that the proposed UWB-based platform can deliver distance estimates with errors below 10 cm for most control points and not exceeding 20 cm for the remaining ones, except for two locations affected by strong multipath. Larger deviations observed at selected locations (e.g., around 12 m and 18 m) show that multipath propagation and local architectural features remain important sources of residual error. Comparable accuracy levels and error patterns have been reported for industrial and logistics-oriented UWB indoor positioning systems operating in complex, cluttered environments [4,8].

From a hardware perspective, the use of 0201 components and four-layer PCBs made it possible to integrate UWB, Bluetooth and environmental sensing into compact anchor and tag designs while preserving adequate RF performance. The overall energy consumption of the tags is strongly dependent on the duty cycle and motion profile of the tracked assets, which follows directly from the motion-triggered activation strategy. The adopted motion-triggered activation strategy, based on an on-board accelerometer and a low-power PMIC, follows a broader trend towards event-driven sensing in warehouse management systems and IIoT tracking solutions, in which only logistically relevant movements are recorded to limit unnecessary transmissions and computations [1].

The observed differences between individual tags at a reference distance of 120 cm illustrate the sensitivity of UWB front-ends to assembly quality, impedance matching and antenna layout. Such variability between nominally identical devices is an important practical limitation when scaling up deployments and may bias system-wide calibration if not properly controlled. A similar emphasis on hardware repeatability and sensor calibration can be found in industrial sensing modalities such as electrical and capacitance tomography, where reconstruction quality and energy efficiency depend simultaneously on sensor design and algorithmic choices [16].

The application of a one-dimensional Kalman filter to distance time series led to a substantial reduction of the RMS error and a marked improvement of the SNR, with particularly strong gains at several distances. These results show that even a relatively simple filtering scheme can significantly stabilize UWB ranging in the presence of high-frequency noise and occasional outliers. At the same time, the slight deterioration at one distance demonstrates the sensitivity of Kalman filters to the choice of process and measurement noise parameters as well as initial conditions, an issue widely discussed in the context of indoor navigation and sensor fusion [39].

Another important limitation of the current approach is the assumption of linear system dynamics and a low-dimensional state vector limited to distance and velocity. While sufficient for the one-dimensional time series analysed in this work, more complex logistics scenarios – involving higher tag velocities, frequent NLOS transitions and dense anchor layouts – will likely require nonlinear filtering strategies and tighter coupling with inertial measurements. The literature on advanced UWB-based indoor positioning and sensor fusion suggests that such extensions can markedly improve robustness in challenging industrial environments [8,39].

Finally, the conceptual link to digital, tomography-like diagnostic chains in non-destructive testing and process monitoring is not only illustrative but also methodologically relevant. In electrical and capacitance tomography, the co-design of sensor geometry, acquisition protocol and reconstruction algorithms has led to substantial gains in energy efficiency and diagnostic performance [16]. By analogy, similar data-centric and energy-aware design patterns can be adopted in UWB indoor tracking by jointly optimizing anchor placement, tag duty cycles, ranging protocols and filtering pipelines, so as to balance positioning accuracy, scalability and maintenance effort in asset-intensive logistics systems.

CONCLUSIONS

Based on the design and experimental evaluation of the proposed UWB-based tracking platform, the following conclusions can be drawn.

The developed hardware-software architecture, comprising custom four-layer anchor and tag PCBs with integrated UWB, Bluetooth and environmental sensing, has proven suitable for indoor asset tracking in warehouse and production-like environments. The combination of PoE-powered anchors and motion-triggered activation of battery-powered tags enables low-maintenance deployment and multi-month operation while preserving tracking continuity.

The calibration and measurement campaign in a 28 m indoor corridor demonstrated that, after antenna-path correction, distance estimates obtained with the TWR method deviate by less than 10 cm for most control points and do not exceed 20 cm for the remaining ones, with larger deviations occurring only at selected locations dominated by multipath effects.

Applying a one-dimensional Kalman filter to the distance time series reduces the mean RMS error from 81.19 cm to 25.63 cm and improves the SNR by about 10 dB, confirming that even a relatively simple filtering scheme can substantially stabilise UWB ranging in realistic indoor conditions.

The current solution is limited by the use of a linear Kalman model with manually tuned noise parameters and a purely distance-based state vector, which motivates future work on adaptive and nonlinear filtering combined with inertial measurements, enhanced NLOS detection and systematic optimisation of anchor layouts for complex industrial buildings.

Overall, the presented platform provides a promising basis for scalable, energy-efficient UWB asset tracking systems that can be integrated with modern warehouse management and production control solutions.

REFERENCES

1. Khan MG, Ul Huda N, Uz Zaman UK. Smart warehouse management system: Architecture, real-time implementation and prototype design. Machines 2022;10:150. https://doi.org/10.3390/MACHINES10020150
2. Che F, Ahmed A, Ahmed QZ, Zaidi SAR, Shakir MZ. Machine learning based approach for indoor localization using ultra-wide bandwidth (uwb) system for industrial internet of things (iiot). 2020 International Conference on UK-China Emerging Technologies, UCET 2020 2020. https://doi.org/10.1109/UCET51115.2020.9205352
3. Niu Z, Yang H, Zhou L, Farag Taha M, He Y, Qiu Z. Deep learning-based ranging error mitigation method for UWB localization system in greenhouse. Comput Electron Agric 2023;205:107573. https://doi.org/10.1016/J.COMPAG.2022.107573
4. Gnaś D, Majerek D, Styła M, Adamkiewicz P, Skowron S, Sak-Skowron M, et al. Enhanced indoor positioning system using ultra-wideband technology and machine learning algorithms for energy-efficient warehouse management. Energies (Basel) 2024;17:4125. https://doi.org/10.3390/EN17164125
5. Li Y, Gao Z, Yang C, Xu Q. A novel UWB/INS tight integration model based on ranging offset calibration and robust cubature Kalman filter. Measurement 2024;237:115186. https://doi.org/10.1016/J.MEASUREMENT.2024.115186
6. Ji P, Duan Z, Xu W. A combined UWB/IMU localization method with improved CKF. Sensors 2024;24:3165. https://doi.org/10.3390/S24103165
7. Zhao W, Goudar A, Tang M, Schoellig AP. Ultra-wideband Time Difference of Arrival Indoor Localization: From Sensor Placement to System Evaluation 2024:2024.
8. Jang B, Kim H, Kim J wook. Survey of landmark-based indoor positioning technologies. Information Fusion 2023;89:166–88. https://doi.org/10.1016/J.INFFUS.2022.08.013
9. Elsanhoury M, Makela P, Koljonen J, Valisuo P, Shamsuzzoha A, Mantere T, et al. Precision positioning for smart logistics using ultra-wideband technology-based indoor navigation: a review. IEEE Access 2022;10:44413–45. https://doi.org/10.1109/ACCESS.2022.3169267
10. Wang K, Yang C. Analysis of machine learning-based NLOS signal identification algorithm for uwb indoor localization using CIR waveform features. The International Archives of the Photogrammetry, Remote Sensing and Spatial Information Sciences 2024;XLVIII-4–2024:705–10. https://doi.org/10.5194/ISPRS-ARCHIVES-XLVIII-4-2024-705-2024
11. Olejniczak A, Blaszkiewicz O, Cwalina KK, Rajchowski P, Sadowski J. LOS and NLOS identification in real indoor environment using deep learning approach. Digital Communications and Networks 2024;10:1305–12. https://doi.org/10.1016/J.DCAN.2023.05.009
12. Al-Okby MFR, Junginger S, Roddelkopf T, Thurow K. UWB-based real-time indoor positioning systems: a comprehensive review. Applied Sciences 2024;14:11005. https://doi.org/10.3390/

APP142311005

13. Rose JL. Ultrasonic Guided Waves in Solid Media 2014;9781107048959:1–512. https://doi.org/10.1017/CBO9781107273610
14. Practice for Radiographic Examination Using Digital Detector Arrays. West Conshohocken, PA: ASTM International; 2018. https://doi.org/10.1520/E2698-18E01
15. Blitz J. Electrical and Magnetic Methods of Non-destructive Testing 1997;3. https://doi.org/10.1007/978-94-011-5818-3
16. Wajman R. The concept of 3D ECT system with increased border area sensitivity for crystallization processes diagnosis. Sensor Review 2021;41:35–45. https://doi.org/10.1108/SR-10-2019-0254
17. Wajman R, Nowakowski J, Łukiański M, Banasiak R. Machine learning for two-phase gas-liquid flow regime evaluation based on raw 3D ECT measurement data. Bulletin of the Polish Academy of Sciences: Technical Sciences 2024;72. https://doi.org/10.24425/BPASTS.2024.148842
18. Grosse CU, Ohtsu M. Acoustic emission testing: Basics for research-applications in civil engineering. acoustic emission testing: basics for research-applications in civil engineering 2008:1–404. https://doi.org/10.1007/978-3-540-69972-9.
19. Zhang K, Entezari A. Convolutional forward models for x-ray computed tomography. SIAM J Imaging Sci 2023;16:1953–77. https://doi.org/10.1137/21M1464191
20. Soleimani M, Rymarczyk T, Klosowski G. Ultrasound brain tomography: comparison of deep learning and deterministic methods. IEEE Trans Instrum Meas 2023. https://doi.org/10.1109/TIM.2023.3330229
21. Koulountzios P, Rymarczyk T, Soleimani M. Ultrasonic time-of-flight computed tomography for investigation of batch crystallisation processes. Sensors 2021;21:639. https://doi.org/10.3390/S21020639
22. Kulisz M, Kłosowski G, Rymarczyk T, Słoniec J, Gauda K, Cwynar W. Optimizing the neural network loss function in electrical tomography to increase energy efficiency in industrial reactors. Energies (Basel) 2024;17:681. https://doi.org/10.3390/EN17030681
23. Kłosowski G, Rymarczyk T, Niderla K, Kulisz M, Skowron Ł, Soleimani M. Using an LSTM network to monitor industrial reactors using electrical capacitance and impedance tomography – a hybrid approach. Eksploatacja i Niezawodnosc 2023;25. https://doi.org/10.17531/EIN.2023.1.11
24. Korzeniewska E, Gałązka-Czarnecka I, Sekulska-Nalewajko J, Gocławski J, Dróżdż T, Kiełbasa P. Assessment of changes in vitamin content and morphological characteristics in strawberries modified with a pulsed electric field using chromatography and optical coherence tomography. NFS Journal 2025;38. https://doi.org/10.1016/J.NFS.2025.100217
25. Rząsa MR. Selection of optical tomography parameters for gas bubble shape analysis. Chemical and Process Engineering - Inzynieria Chemiczna i Procesowa 2014;35:19–33. https://doi.org/10.2478/CPE-2014-0002
26. Przysucha B, Wójcik D, Rymarczyk T, Król K, Kozłowski E, Gąsior M. Analysis of reconstruction energy efficiency in EIT and ECT 3D tomography based on elastic net. Energies (Basel) 2023;16. https://doi.org/10.3390/EN16031490
27. Rymarczyk T, Niderla K, Kozłowski E, Król K, Wyrwisz JM, Skrzypek-Ahmed S, et al. Logistic regression with wave preprocessing to solve inverse problem in industrial tomography for technological process control. Energies (Basel) 2021;14:8116. https://doi.org/10.3390/EN14238116
28. Rząsa M. Assessment of benefits resulting from the use of computer control systems in precision agriculture. Bulletin of the Polish Academy of Sciences Technical Sciences 2023:144582–144582. https://doi.org/10.24425/BPASTS.2023.144582
29. Rzasa MR, Czapla-Nielacna B. Analysis of the influence of the vortex shedder shape on the metrological properties of the vortex flow meter. Sensors 2021;21. https://doi.org/10.3390/S21144697
30. Van Herbruggen B, Gerwen JV Van, Luchie S, Durodie Y, Vanderborght B, Aernouts M, et al. Selecting and combining UWB localization algorithms: Insights and recommendations from a multi-metric benchmark. IEEE Access 2024;12:16881–901. https://doi.org/10.1109/ACCESS.2024.3358274
31. Krawczyk A, Korzeniewska E. Some aspects of electromagnetic field shielding. Przeglad Elektrotechniczny 2023;99:128–31. https://doi.org/10.15199/48.2023.03.22
32. Gao X, Sadjadpour HR, Dowla FU, Nekoogar F. Optimal communication system with power control and ultra-wideband propagation channel model designs for monitoring harsh through-wall environments. IEEE Access 2024;12:56226–39. https://doi.org/10.1109/ACCESS.2024.3389681
33. Al-Okby MFR, Junginger S, Roddelkopf T, Thurow K. UWB-based real-time indoor positioning systems: a comprehensive review. Applied Sciences 2024;14:11005. https://doi.org/10.3390/APP142311005
34. Chen Y, Wang J, Yang J. Exploiting Anchor Links for NLOS Combating in UWB Localization. ACM Trans Sens Netw 2024;20. https://doi.org/10.1145/3657639/ASSET/939C25F8-3F32-4CA9-840D-CFBD7EF6B394/ASSETS/IMAGES/LARGE/TOSN-2023-0444-F17.JPG
35. Wang F, Tang H, Chen J. Survey on NLOS identification and error mitigation for UWB indoor

positioning. Electronics (Basel) 2023;12:1678. https://doi.org/10.3390/ELECTRONICS12071678

36. Kerr CC, Dura-Bernal S, Smolinski TG, Chadderdon GL, Wilson DP. Optimization by adaptive stochastic descent. PLoS One 2018;13:e0192944. https://doi.org/10.1371/JOURNAL.PONE.0192944
37. Wymeersch H, Maranò S, Gifford WM, Win MZ. A machine learning approach to ranging error mitigation for UWB localization. IEEE Transactions on Communications 2012;60:1719–28. https://doi.org/10.1109/TCOMM.2012.042712.110035
38. Gurin D, Yevsieiev V, Abu-Jassar A, Maksymova S. Using the Kalman filter to represent probabilistic models for determining the location of a person in collaborative robot working area. Multidisciplinary Journal of Science and Technology 2024;4:66–75.
39. Lu N, Gao Z. Ultra Wideband indoor positioning method based on Kalman filter and Taylor algorithm. 2022 4th International Conference on Intelligent Control, Measurement and Signal Processing, ICMSP 2022 2022:910–4. https://doi.org/10.1109/ICMSP55950.2022.9859227
40. Li Y, Gao Z, Yang C, Xu Q. A novel UWB/INS tight integration model based on ranging offset calibration and robust cubature Kalman filter. Measurement 2024;237:115186. https://doi.org/10.1016/J.MEASUREMENT.2024.115186
41. Lv H, Liu M, Liu P, Chang K, Li M, Piao C. Kalman filter-based high-accuracy indoor positioning with NLoS error mitigation and multi-motion model switching. IEEE Trans Veh Technol 2025;74:12673–88. https://doi.org/10.1109/TVT.2025.3556393